Thunder acoustic signature for channel reconstruction in triggered lightning

Jianguo Wang; Jinxin Cao ✉ ; Li Cai; Rui Su ; Mi Zhou; Yadong Fan; Quanxin Li

Check for updates

View Online   Export Citation

Articles You May Be Interested In

The characteristics of thunder on Titan.

J Acoust Soc Am (March 2010)

The propagation of thunder through the atmosphere

J Acoust Soc Am (June 1980)

Modeling thunder propagation and detectability on Titan.

J Acoust Soc Am (April 2011)

06 January 2025 07:00:25

Thunder acoustic signature for channel reconstruction in triggered lightning EP

View Online   Export Citation   CrossMark

Jianguo Wang,[1] Jinxin Cao,[1,2,a] Li Cai,[1,b] Rui Su,[1] Mi Zhou,[1] Yadong Fan,[1] and Quanxin Li[1]

AFFILIATIONS

[1]School of Electrical Engineering and Automation, Wuhan University, Wuhan, China
[2]Department of Building Environment and Energy Engineering, The Hong Kong Polytechnic University, Hong Kong, China

[a]Author to whom correspondence should be addressed: jinxin.cao@connect.polyu.hk
[b]cail@whu.edu.cn

ABSTRACT

There are few reports on the near-field acoustic signals corresponding to lightning return strokes. One rocket-triggered lightning flash, which contains 13 return strokes, initial continuous current (ICC) processes, and abundant M-components, was observed in the summer of 2018 and reported in this study. The complete near-field acoustic pressure signals initiated by the flash were recorded and analyzed. It is found that the near-field acoustic pressure signals from each return stroke are composed of the first arrived N-shape shock waveform and the subsequent low-frequency oscillating waveforms. The characteristic of the acoustic waveforms has been parametrically defined and quantitatively analyzed, with a comprehensively acoustic-electrical correlation investigation. The acoustic pressure signals from intensive ICC processes and M-component pulses with different discharge intensities are also discussed. It is found that the too-close time interval between M-component and previous current pulses would affect the generation and measurement of the acoustic pressure waveforms from the M-component, even though the discharge amplitude is competitive and the wavefront is fast. The same phenomenon has also been observed in the acoustic signals from a return stroke with a too close interval from the previous pulse. The acoustic source localization with great accuracy for lightning channel reconstruction was realized based on the measured acoustic signals. The reconstructed channel structure agrees with that of the synchronously captured optical image. The study of the characteristics of acoustic signals from lightning discharge contributes to the recognition of thunder signals, source localization for channel reconstruction, and understanding of the lightning discharge process.

06 January 2025 07:00:25

I. INTRODUCTION

Natural lightning is a strong instantaneous discharge process, accompanied by the generation of multiple physical radiations with sound, light, and electromagnetic waves. Thunder radiation is the result of the propagation of shock waves caused by the rapid expansion of air around lightning channels.[1] Acoustic monitoring is a widely used research method in scientific and industrial circles. Quantitative observation of the lightning acoustic signal will contribute to the study of thunder radiations, source localization for discharge-channel reconstruction, and understanding of the mechanisms of the lightning discharge process.

In the literature, single-station or multi-station outdoor acoustic detections were carried out with microphone arrays containing audible or infrasound frequency bands of thunder signals. Regarding lightning flash as a whole event, the characteristics of thunder sound in both the time-domain and frequency-domain,[2–4] propagation in atmospheric thunderstorm,[5–8] and acoustic location[9–12] were reported. However, there are few reports on the characteristics of lightning acoustic pressure signals corresponding to the return strokes (RSs) in the lightning flash. The characteristic of near-field acoustic pressure signals from lightning flashes has been not well observed and addressed.

Considering the high efficiency of triggered-lightning flashes,[13] both electrical and near-field acoustic observations of rocket-triggered lightning flashes were carried out in Guangdong, China in the summer of 2018.[14–18] A rocket-triggered lightning flash, which contains 13 return strokes, abundant ICC process, and M-component pulses, was reported in this study. The complete near-field acoustic pressure signals initiated from a lightning flash have been described.

The near-field acoustic pressure signals corresponding to each return stroke are found to be composed of the first arrived N-shape shock waveform and the subsequent low-frequency acoustic waveforms. Note that the phenomenon has not been found in the past acoustic observations on both natural lightning[2,19,20] and triggered lightning flashes[21,22] reported before.

In this study, the characteristic of the acoustic pressure signals has been investigated with new parametric definitions and a detailed correlation analysis of the acoustic-electrical parameters. Meanwhile, the acoustic signals corresponding to intensive ICC processes and M-component pulses are given and further analyzed. The factor that affects the generation and measurement of the acoustic waveforms initiated from the M-component is also discussed. Based on the measured acoustic signals, the acoustic radiation localization from the lightning return stroke channel was realized. The reconstructed channel structure by the localized acoustic sources was compared with the captured optical image.

This paper is organized as follows: The following section is the introduction of the experimental observation and the technique of the acoustic localization algorithm. Section III is the analysis of the observed results. The observed complete acoustic pressure signals are first described. The first arrived acoustic N-shape shock waveforms, the subsequent acoustic low-frequency oscillating waveforms, and the acoustic pressure signals of the other discharge processes, i.e., the ICC process and M-component are then investigated. The localization results of acoustic radiations are further reported. Finally, the discussion and the conclusion are respectively presented in Secs. IV and V.

II. METHODS

A . Layout of the experiment site

In the summer of 2018, an experiment of rocket-triggered lightning comprehensive observation had been established in Conghua, Guangzhou Province, China. A rocket launcher that can lead the triggered-lighting flash to terminate on both ground and 10 kV distribution lines were built in the experiment field. Figure 1(a) shows a map that presents the overall location of the observing experiment and the distance from the optical observing site to the experiment field. The optical observing site is equipped with a high-speed camera to record the discharge channel of triggered lightning, located at a distance of 1.6 km from the rocket launch point. The optical camera is set up on the roof of a 5-story residential building, so there is almost no obstruction in the line of sight. Figure 1(b) shows the top-view photograph of the experiment field and presents the locations of the acoustic array, as well as the rocket launcher. The acoustic array was installed 130 m away from the rocket launcher. Note that most of the area in and around the field is flat, with only a small number of trees.

B. Measuring equipment

The current signals from each flash were measured at the lightning channel base by both coaxial shunt and Rogowski coil. The signals are transmitted by an optical-electric conversion device to ensure the quality of data. The signals would also be simultaneously distributed to the launch control room (LCR) as the trigger condition for a multichannel oscilloscope. The LCR integrates the function of multi-parameter observation for rocket-triggered lightning by acoustic, optical, and electromagnetic sensors installed in the near field. The appearance of the LCR is shown in Fig. 1(c). The red dots mark the orthogonally placed four microphone sensors with a base length of $5 \times 2 \times 1.2$ m, which were installed on the top of the three metal poles. To minimize the effects of environmental interference on acoustic observation, the acoustic sensors were set up with metal thin rods at a position 5 m above the ground. The sensor integrated a constant current power preamplifier with a frequency response of 10 Hz–20 kHz and a dynamic range of more than 130 dB. A wind ball, outer shell, and thin film were used to reduce the ambient wind noise and rainwater interference. It has been found through an indoor test that the sensor's response waveform is hardly affected, with an attenuation of the decibel response of within 3 dB.
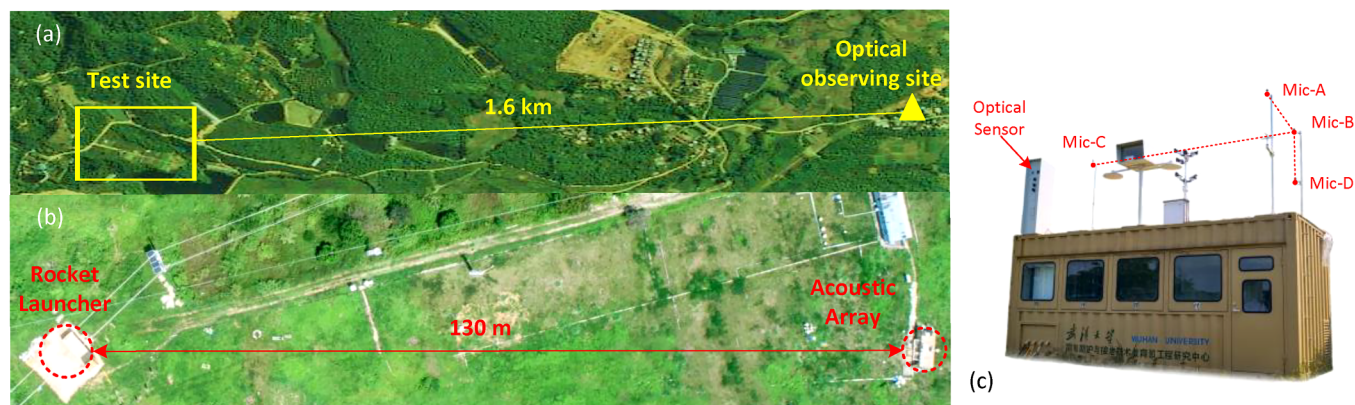

FIG. 1. (a) Map of the location of the optical observing site (b) Top-view photograph of the experiment field for rocket-triggered lightning. (c) Diagram of the microphone acoustic array.

In the observation, the lightning acoustic signals recorded by the sensors were transmitted by shielded cables to the digital acquisition system installed in the LCR. The acquisition system is equipped with a four-channel NI-DAQ card with a maximum sampling rate of 102.5 kS/s. The system was triggered by an external optical sensor, as shown in Fig. 1(c). The optical sensor responds quickly to the changes in light intensity caused by rocket-triggered lightning flash and then outputs transistor-transistor logic (TTL) signals of 2 V.

C. Localization algorithm

For acoustic source localization, after the array acquisition of original acoustic signals, the continuous time-domain signals will be pre-processed and separated into segments. The time difference arriving at the microphone array is calculated based on the cross-correlation algorithm. The parameters, including incidence angles Az, El, and the absolute distance r from the acoustic source to the central microphone (Mic-B), are defined for the localization.

The diagram of the spatial geometric relation for a single acoustic source with the observing microphone array is shown in Fig. 2(a). The theoretic equations for localization based on the observed arriving time delay are illustrated following.

First, we establish the plane coordinate system A-B-C formed by the connecting lines A-to-B and B-to-C between the microphones, as shown in Fig. 2(a). For acoustic source localization, the angles between the incident vector $\overrightarrow{OB}$ and the coordinate axis, i.e., Θ_1 and Θ_2, need to be adopted. The geometric relationship between each angle and the defined lines in Fig. 2(a) could be represented by the equations as follows:

$$\begin{cases} \cos(\theta_1) = BO_{bc}/r, \\ \cos(\theta_2) = BO_{ab}/r, \\ \cos(El) = B\grave{O}/r, \\ \cos(Az) = BO_{bc}/B\grave{O}, \\ \tan(Az) = \grave{O}O_{bc}/BO_{bc} = BO_{ab}/BO_{bc}. \end{cases} \quad (1)$$
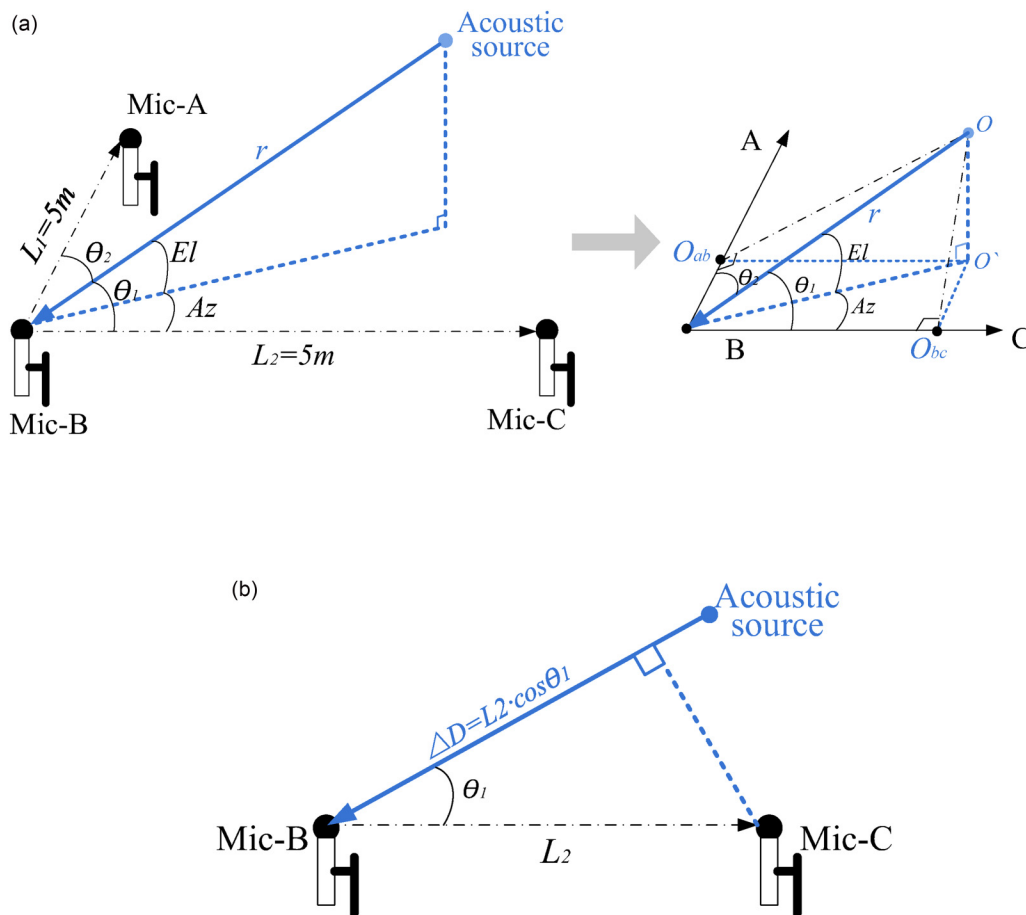

FIG. 2. Diagram of (a) the geometric relationship between sound source direction and acoustic array. (b) The geometric relationship related to Θ_l.

Combining the 1st, 2nd, and the 5th equation in (1), the calculation of Az and El can be described as follows:

$$\begin{cases} Az = \tan^{-1}(\cos(\theta_2)/\cos(\theta_1)), \\ El = \cos^{-1}(\cos(\theta_1)/\cos(Az)). \end{cases} \quad (2)$$

Then, assuming the acoustic radiation that propagates to the microphone array as a plane wave, because of the small size of the microphone array, the geometric relationship related to Θ_1 and Θ_2 is shown in Fig. 2(b). Thus, the Θ_i could be calculated as below,

$$\cos(\theta_i) = \Delta D_i / L_i, \quad (3)$$

where ΔD_i is the travel difference between the acoustic wave arriving at the A/C and arriving at B. ΔD_i corresponds to the time delay of arriving at different microphones, which matches the

relationship below,

$$\begin{aligned} \Delta t_{ij\_r} &= t_{i\_r} - t_{j\_r}, \\ \Delta D_i &= \Delta t_{ij\_r} \cdot v, \end{aligned} \quad (4)$$

where Δt_{i_r} and Δt_{j_r}, respectively, represent the arrival time to a particular microphone i and j. Δt_{ij_r} represents the difference in the time arriving the microphones i and j. v is the velocity of an acoustic wave propagating in an atmospheric environment and adopted as 347 m/s at a temperature of 25 °C. The least-square method is adopted to find the correct Δt_{ij_r} which is closest to the actual Δt_{ij} of the signal segment of acoustic pressure waves to find the correct incident angle by Eqs. (2)–(4). After the incidence angles, i.e., Az_r and El_r were calculated, the corresponding direction of the acoustic source could be obtained. Combined with the arrival time Δt_{B_r}, the spatial position of acoustic radiation could be obtained
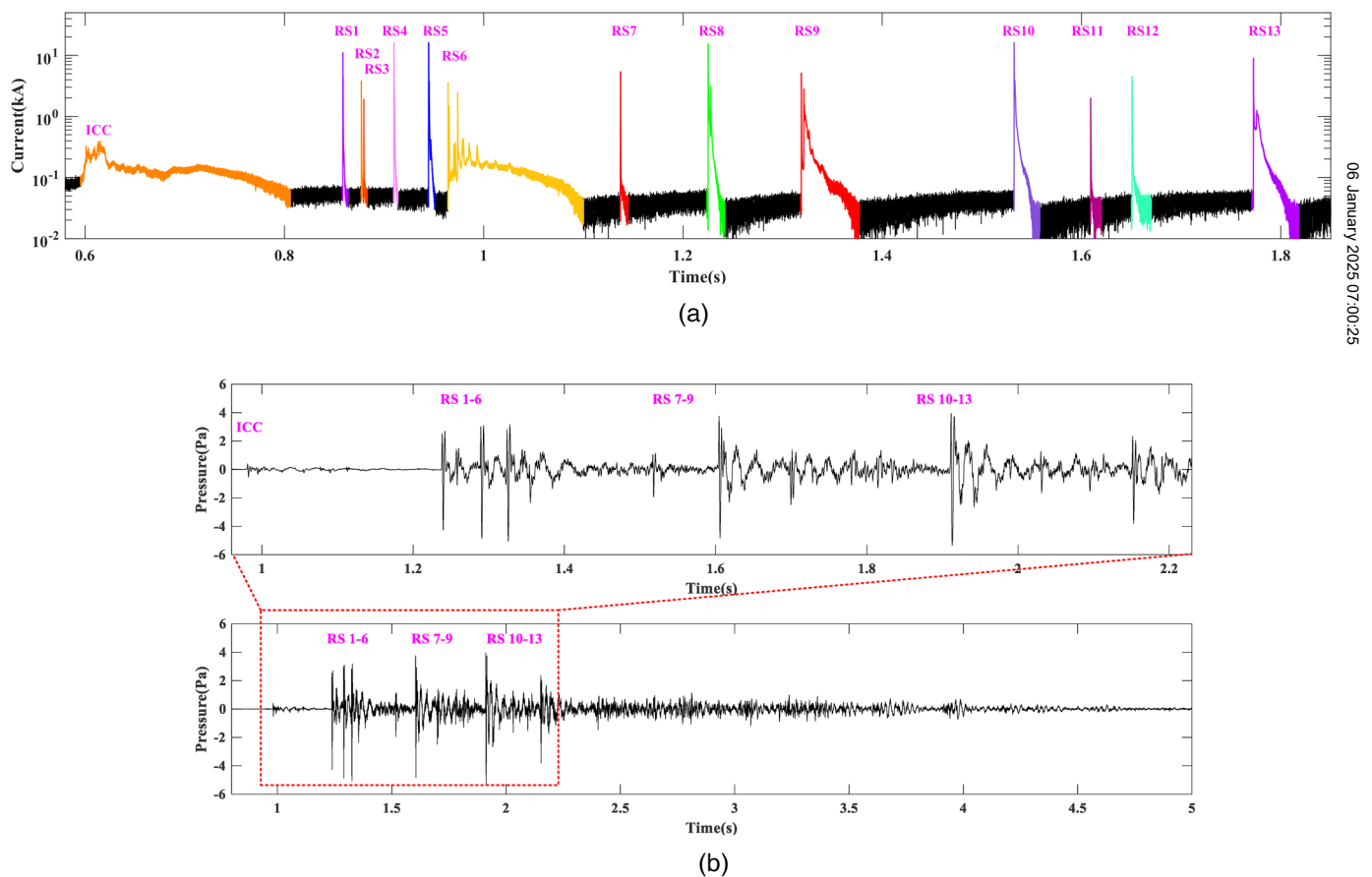

FIG. 3. Synchronous observed: (a) current signals. (b) A complete acoustic pressure signals recorded for the triggered lighting flash, with the partial acoustic pressure signals presented with the same time scale as that of the (a) current signal.

as S (r, El_r, Az_r), with the radial distance calculated below,

$$r = t_{B\_r} \cdot v. \tag{5}$$

III. RESULTS

A. Observed complete acoustic pressure signals

On July 26, 2018, a rocket-triggered negative lightning flash which includes 13 return strokes (RSs), rich initial continuing current (ICC) pulses, and M-components occurred and was successfully observed at 14:11:16 pm. Figure 3 illustrates the synchronous current signal and the acoustic pressure signals recorded for the flash. In Fig. 3(a), different colors are used to highlight the current pulse corresponding to each return stroke process. The peak current (I_{max}) of the RSs ranges from 6.54 to 32.88 kA, with a mean value of 18.98 kA.

Shown in the lower part of Fig. 3(b) is the complete acoustic pressure signals recorded for the triggered lighting flash. It is found that the main pressure signals initiated by different lightning discharge processes appear as a distinct cluster of high-amplitude pulses. Note that the bottom of the lightning channel is a nearly vertical channel guided by steel wire combustion. The thunder radiations initiated from this part could be easily distinguished without the superposition of other acoustic sources. Therefore, the time-delay relationship of the acoustic–electric pulses can be easily matched with each other, including the acoustic waveforms corresponding to the ICC process, RS process, reflection, and farther acoustic source. The partial acoustic pressure signals presented with the same time frame as that of the current signals in Fig. 3(a) are also presented, as shown in the upper part of Fig. 3(b). It could be found in Fig. 3(b) that the recorded first arrived acoustic pressure waveform of each discharge process always has a higher amplitude than the acoustic signals around, and it can match the relative time-delay relationship to that of the current pulses. Note that the synchronously triggered acoustic acquisition system can only record the acoustic pressure signals after a propagation time delay due to the observing distance of 130 m from the lightning channel. Thus, the timescale of the recorded acoustic signals has an obvious time delay, compared to the timescale of the current signals.

The acoustic pressure signals of each return stroke under the 100 ms time window, as well as the corresponding frequency-domain power spectra obtained by S-domain transformation,[23] are shown in Fig. 4. The arrival time delay of near-field acoustic waves is approximately equal to the linear propagation time from the rocket launch to the acoustic measuring array. The first subgraph shows the signal section before the first obvious pressure waveform, which is considered to be the background noise before the thunder arrives. The absolute amplitude is extremely low, with a ratio of the amplitude to the obvious pulse that first arrives in the echo process of less than 1%. Therefore, the obtained acoustic signals of the thunder radiations have a high signal-to-noise ratio.

Seeing the partial time-domain waveforms in Fig. 4, it is found that the obvious shock waveform (blue marker) is the first one to be measured and initiated from a single return stroke process, which is similar to the results reported.[21,22] Note that the shape of the first arrived acoustic shock waveform from the RS

process is a bit like the shape of the letter "N," thus it is called the "N-shape waveform" in this study. Furthermore, it is observed that subsequently following the acoustic N-shape waveform is the waveform that lasts tens of milliseconds, while its amplitude and frequency are much lower (marked by red, called the "low-frequency band" in this study). The amplitude and frequency of the acoustic low-frequency band gradually attenuate after several cycles until a weak amplitude without obvious characteristic changes (green mark, labeled as "weak band" in this study). It is also found that if the time interval between the return strokes is short, the weak band will not appear and the first arrived acoustic N-shape waveform corresponding to the next return stroke is always directly superimposed on the previous low-frequency band.

The S-domain transform spectra in Fig. 4 corresponding to the observed acoustic waveforms reflect the frequency components and relative intensity of acoustic signals in each discharge process. The normalized intensity, based on the maximum value of the acoustic signals, is represented by the color map. The peak frequency of the first arrived N-shape waveforms is between 200 and 400 Hz, and the main frequency range (normalized intensity greater than 0.2) is between 200 and 800 Hz. The frequency components of the low-frequency band and the small N-shape waveforms superimposed on it are also reflected on the spectrum. The low-frequency component is found to be tens of hertz, and the frequency of the superimposed small N-wave is roughly similar to that of the first arrived N-shape waveforms.
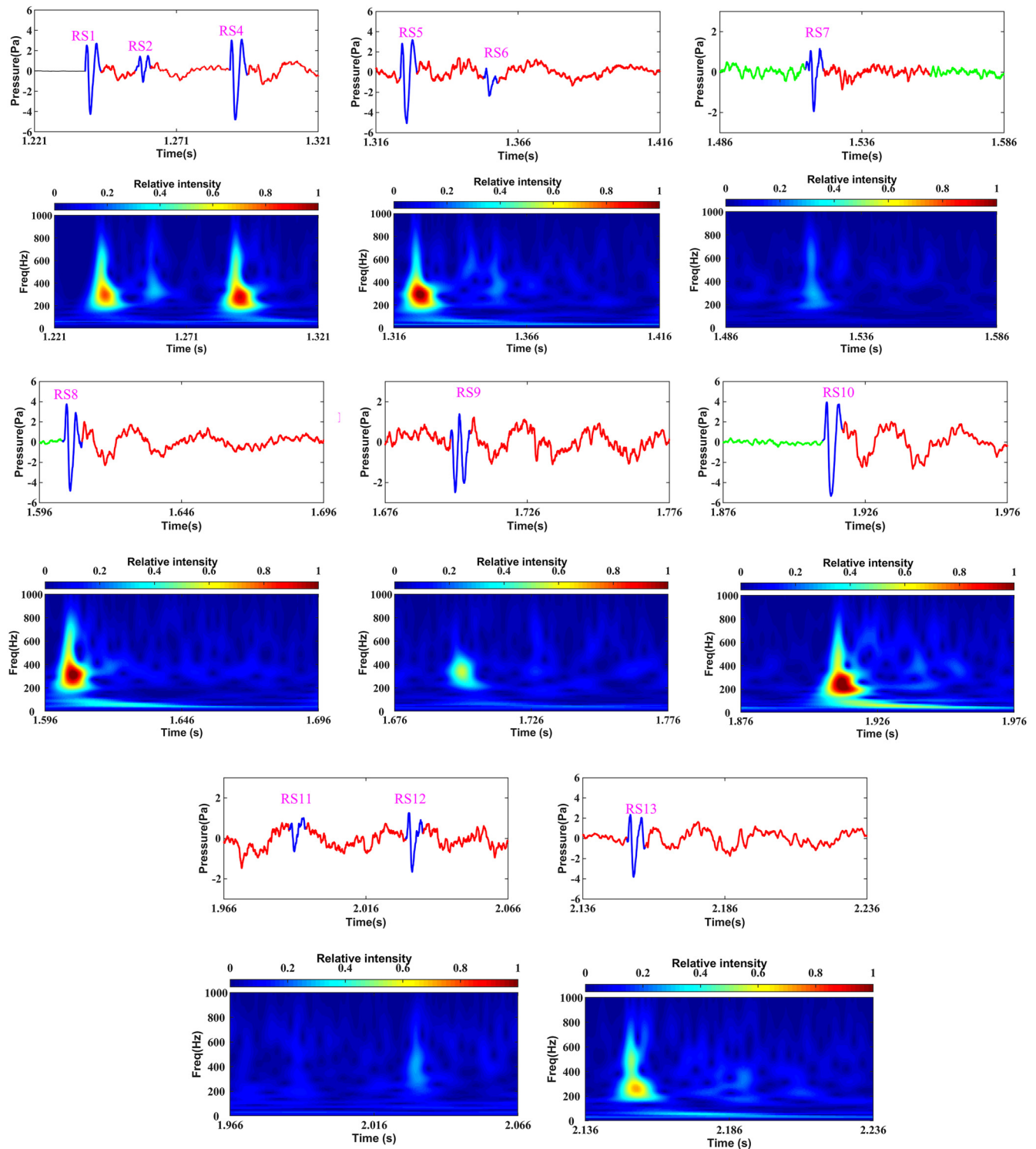
B. The first arrived acoustic N-shape waveform of RS process

Shown in Fig. 5(a) is the first arrived N-shape waveform initiated from a single RS, which begins with overpressure and depression and is then followed by a significant overpressure and depression (sometimes, the amplitude of the second overpressure or depression is not obvious enough, and the amplitude is close to zero). The typical shape is similar to that of the simulated lightning-current discharge in the laboratory.[24] The definition of the characteristic parameters is illustrated in Fig. 5(a), including amplitude parameters P_{1max}, P_{1min}, P_{2max}, P_{2min}, and time parameters T_{1min}, T_i, T_d, and T_r. After the waveform is separated, the acoustic energy/unit volume E_{vol} (J/m^3) could be defined and calculated[21] below,

$$E_{vol} = \frac{\int P(t)^2}{\rho_o c_o^2}, \tag{6}$$

where P_0 and c_0 represent atmospheric pressure density and sound velocity, respectively. The integral range is determined by the delimitation of the first arrived N-shape waveform. Note that P_0 and c_0 are adopted as constant during the process of the lightning flash.

Based on the nine defined characteristic parameters for acoustic N-shape waveforms of RSs, the fitting analysis of acoustic-electrical parameters of the N-shape waveforms vs RS current was carried out to comprehensively investigate the acoustic-electrical correlation. The scatter diagram, fitting curve, coefficient of determination R^2, and corresponding 95% confidence interval of the characteristic parameters are shown in Figs. 5(b)–5(i).

FIG. 4. Acoustic pressure waveforms of each RS under 100ms time scale and the corresponding frequency-domain power spectra obtained by S-domain transformation.
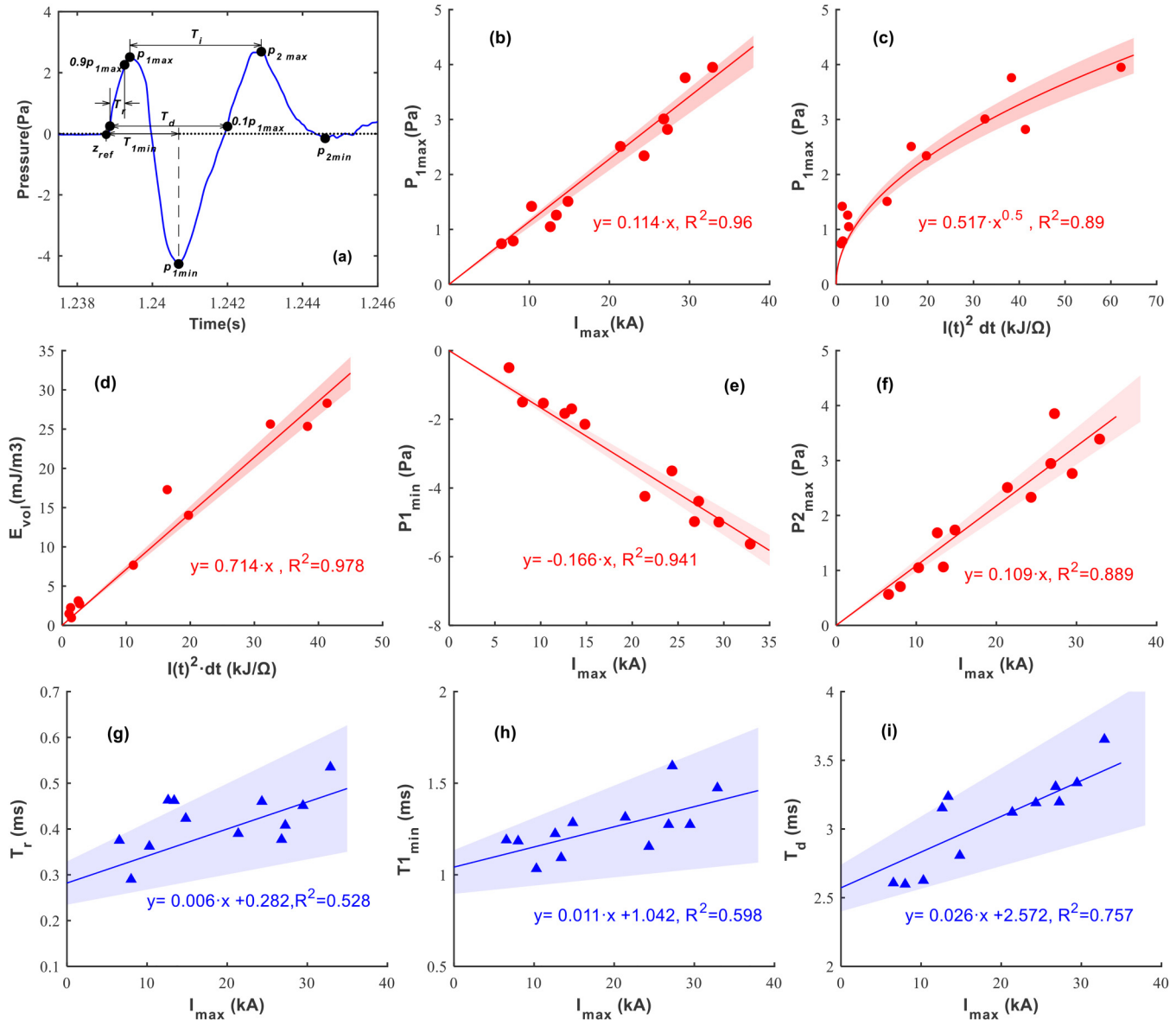
06 January 2025 07:00:25

FIG. 5. (a) The first arrival N-shape waveform initiated from an RS and the definition of acoustic parameters. (b)–(i) The scatter diagram, fitting curve, and 95% confidence interval of the acoustic parameters vs electrical parameters of the RS current pulse.

The fitting of the amplitude and energy parameters were marked in red as shown in Figs. 5(b)–5(f). It is found that the peaks of the first N-shape waveform, i.e., P_{1max}, P_{1min}, P_{2max}, increase linearly with the amplitude of the RS current I_{max}. A good linear relationship could be also found between the energy density E_{vol} vs the specific energy of the RS, the latter of which is calculated by the integral of the current value, i.e., $\int i(t)^2 dt$. The higher fitting degree can be reflected according to the 95% confidence interval and the coefficient of determination R^2. Considering that the

specific energy of the RS is derived from the square integral of the transient value of the current, the power function model is adopted when fitting with acoustic P_{1max}, which also has a high degree of fitting, as shown in Fig. 5(c).

The variation of the three acoustic time parameters with the amplitude of the current was marked in blue as shown in Figs. 5(g)–5(i). It is found that although the time parameters of acoustic waveforms reflect a positive correlation trend with current amplitude I_{max}, the variation degree of parameters is relatively

small, while the linear fitting dispersion is large, as shown in Figs. 5(g)–5(i).

Overall, seven of the nine acoustic parameters defined in the study are related to the increase in electrical parameters. The other two acoustic parameters, P_{2min} and T_{1min}, are not found to have a significant correlation with electrical parameters in statistics. The probable reason is that the statistical P_{2min} fluctuates mainly near-zero value, while T_{1min} fluctuates slightly above and below the mean value. Neither of them reflects the distribution law following the variation of the electrical parameters.

C. The acoustic low-frequency bands of the RS process

Following the first arrived acoustic N-shape waveform is a low-frequency band with a relatively low amplitude, low frequency, and attenuation oscillation. It is shown in Fig. 4 that the N-shape waveform tends to transition to the low-frequency band at the end of the second peak. Unlike the smooth first arrived N-shape waveforms, the low-frequency bands are superimposed with various small and distorted pressure waveforms, which is similar to the phenomenon observed in the natural thunder signals.[2,19,20] These small-amplitude pressure waveforms are regarded to originate from the farther part of the return-stroke channel.

To reveal the waveform characteristics, the amplitude normalization and waveform superposition of the low-frequency bands from various RS processes were carried out, as shown in Fig. 6(a). The cyan part is the superposed low-frequency band and the blue

part is the first N-shape waveform corresponding to an RS. It is found that the relative amplitude characteristics of the positive and negative peaks of each low-frequency cycle wave are similar. That is to say, low-frequency bands of each RS process change according to similar periodic laws, although the duration is different.

Note that for some weak RS processes with a too close time interval from the pre-sequence RS pulse, e.g., RS6 and RS11 shown in Fig. 4, the acoustic N-shape waveforms are directly superimposed on the low-frequency band from the previous RS process. In this case, there is no low-frequency band of their own. It is also noted that the duration of corresponding low-frequency bands is different, due to the randomness of the time delay between various RSs, as well as the superposition effects. The longest low-frequency band is found to be about 100 ms. Those low-frequency bands that end early due to too close intervals may be far less than 100 ms in length.

According to the typical characteristics of the low-frequency band, the peak amplitude and relative time of the three cycles are marked and counted. The six labeled parameters are shown in Fig. 6(a), and the parameters of the recorded low-frequency band corresponding to all the RS processes were extracted. The variation relationship between the amplitude of each acoustic peak and the corresponding relative time delay was shown as scatter points in Fig. 6(b). Different color points reflect the samples of different parameters. It is found that the amplitude of each parameter satisfies the law of exponential decay well with the relative time. Furthermore, Figs. 6(c) and 6(d), respectively, show the correlation fitting between the maximum amplitude of the low-frequency band
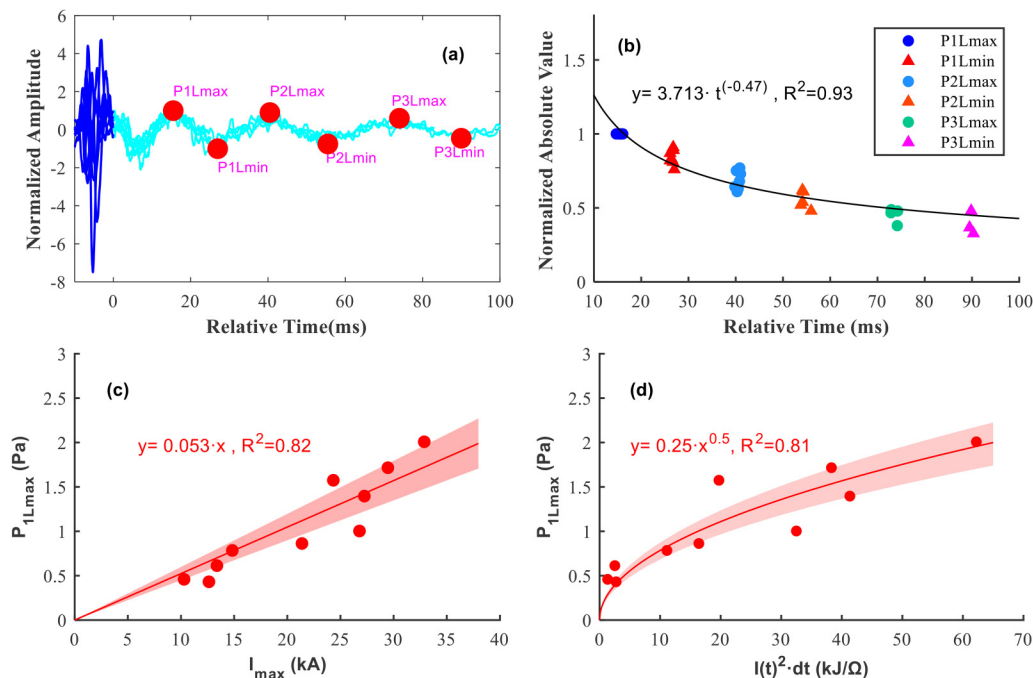

FIG. 6. (a) The amplitude-normalization and superposition of the acoustic low-frequency bands, with characteristic parameters defined. (b) The amplitude of the low-frequency band's each peak vs relative time delay. (c) The first peak's amplitude of the low-frequency band P_{1Lmax} vs the amplitude of RS current I_{max}. (d) The first peak's amplitude of the low-frequency band P_{1Lmax} vs specific energy of the RS current.

and the peak current or specific energy during the return stroke process. A good correlation has been found in the fitting.

D. Acoustic waveforms of initial continuous current pulses

Figures 7(a) and 7(b) show the recorded initial continuous current (ICC) pulses in the flash and the corresponding acoustic pressure signals, respectively. This process of acoustic pressure signals is the first to arrive at the acoustic sensor and is not affected by the superposition of other sound sources. In addition to recording the acoustic pressure signals with the largest amplitude corresponding to ICC pulses, relatively low amplitude and continuous pressure waveforms were also recorded after the first arrival of N-shape waveforms. This part of the acoustic pressure signals may come from the current pulses superimposed on the continuous ICC process, according to the time-delay characteristics. Note that the typical characteristics of ICC pulses in the flash are not obvious to distinguish independently one by one. Thus, there is no good relationship between acoustic N-wave and irregular ICC pulses in terms of both amplitude and time-delay correspondence. After all, the wavefront, duration, and amplitude of the lightning current pulse affect whether the acoustic waveforms can be observed or not.

Note that since the study mainly reported a single lightning flash with limited observed cases of ICC pulses, the typical acoustic features of the ICC discharge process would be further explored in future work.

E. Acoustic waveforms of M-components

In the observed flash, abundant M-component processes after the RS pulses were also recorded, totaling about 19 times. Some typical current waveforms with dense M-components are shown

in Figs. 8(a) and 8(b), i.e., after RS6 and RS9 processes. The M-component lightning current pulses are shown and marked by different colors. Note that the current pulse characteristics are similar to the observations in other rocket-triggered lightning flashes.[25]

The corresponding acoustic pressure signals are plotted on the same time scale as shown in Figs. 8(c) and 8(d). It is found that the one-to-one corresponding acoustic N-shape waveforms from the M-components are difficult to measure. According to the work of,[22] the main conditions for each discharge process to create acoustic radiations are related to the wavefront and amplitude of the discharge pulse. Thus, the probable reason is that the observed M-components usually rise slowly with a measured wavefront longer than 300 μs and have low measured amplitude of less than 1 kA. On the other hand, however, for the M-component pulses at 965, 974, and 1321 ms respectively, their rising time is fast, with a range of 17.9–29.3 μs. Note that their amplitudes are also comparable to the previous RS current pulses, with a value of 1.58, 2.51, and 2.82 kA, respectively. While the corresponding independent acoustic pressure pulse signal was still not measured.

To explain this, it is regarded in this study that the time interval between the three M-components and the previous RS pulses is too close, with all values of less than 10 ms. Considering the mechanism of acoustic-radiation excitation, the lightning ionization channel has not completely dissipated after the thermal expansion of the return channel. In this case, even if there are strong M-components that continue to maintain the channel discharge, the secondary plasma channel would not expand dramatically and initiate a shock wave to form the mechanical sound wave.

The phenomena consistent with the above explanations can also be observed in RS2 and RS3 processes, which also have an extremely small interval, with a value of less than 3 ms. The current waveforms of RS2 and RS3 are shown in Fig. 8(e). Their corresponding acoustic
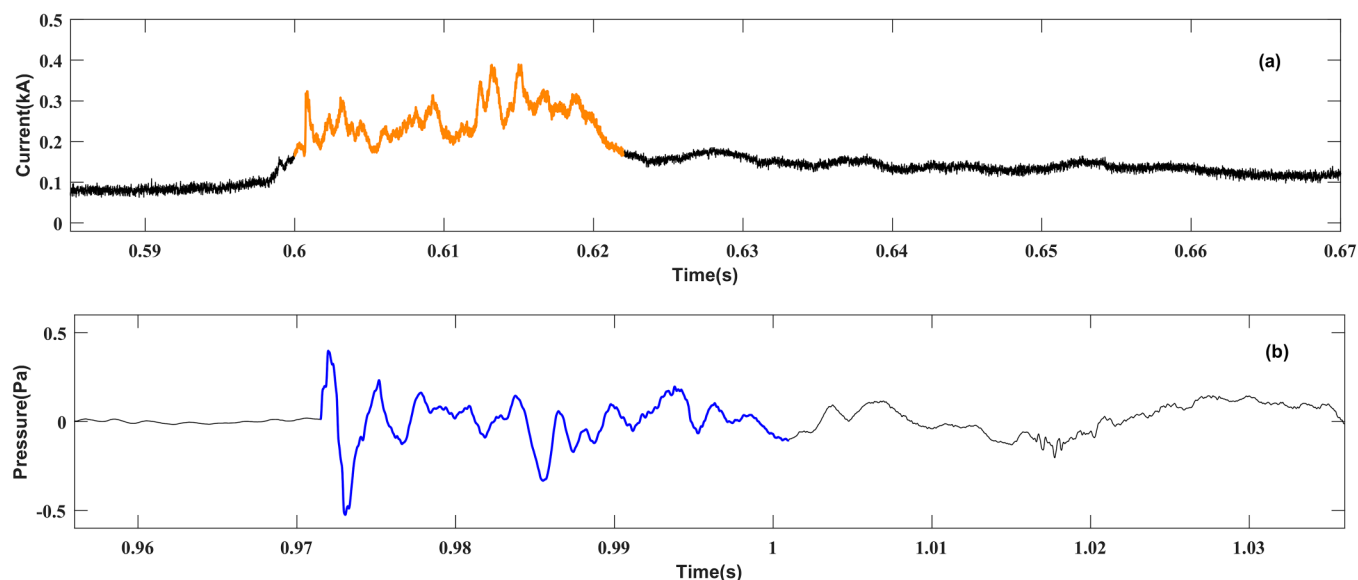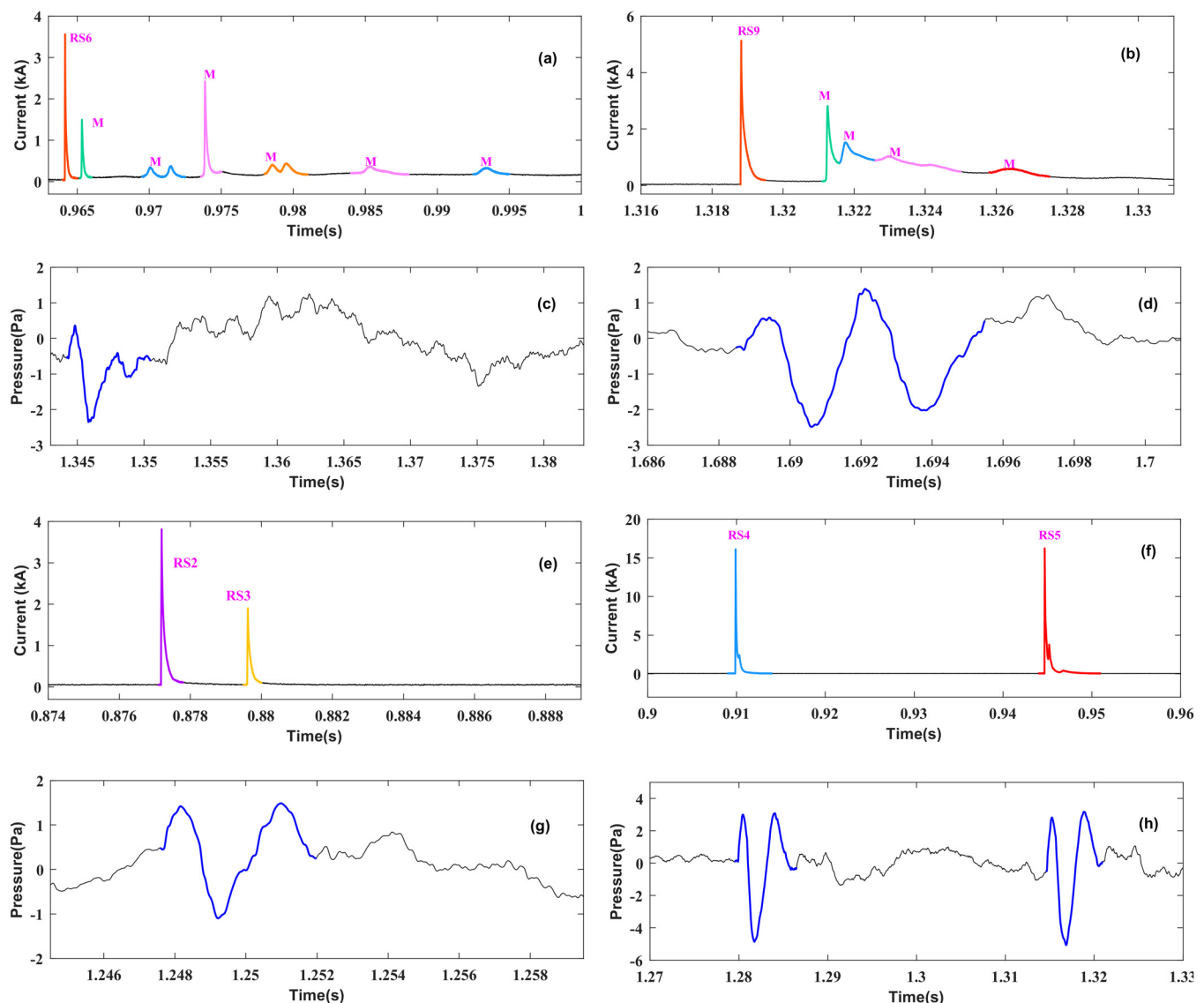

FIG. 7. (a) Current waveforms of ICC pulses. (b) Corresponding acoustic pressure waveforms.

FIG. 8. (a)–(d) Current pulses of RSs with dense M-components and corresponding acoustic pressure waveforms. (e)–(h) The current pulses of RSs with different intervals and their corresponding acoustic pressure waveforms.

waveforms are respectively shown in Fig. 8(g). It is found in Fig. 8(g) that RS3 does not have an obvious independent acoustic N-shape waveform. If the time interval from the previous current pulse is farther, e.g., the RS5 current pulses after the RS4 pulse, as shown in Fig. 8(f) and their acoustic waveforms shown in Fig. 8(h), an independent acoustic N-shape waveform corresponding to the RS5 could be easily found. Therefore, the comparison of the acoustic response of RS3 and RS5 pulses further proves the significant influence of the time interval on acoustic radiation response.

To summarize, the too-close time interval between M-component and previous current pulses significantly affects the generation and

measurement of M-component acoustic pressure waveforms, even though the current amplitude is comparable to that of return stroke and the wavefront is fast. The same phenomenon occurs in the acoustic signals from two return stroke pulses with too close intervals.

F. Acoustic radiations localization for channel reconstruction

Based on the measured acoustic waveforms, the spatial localization of the acoustic radiation sources from the flash for channel reconstruction was realized. Figure 9(a) is an optical image of one
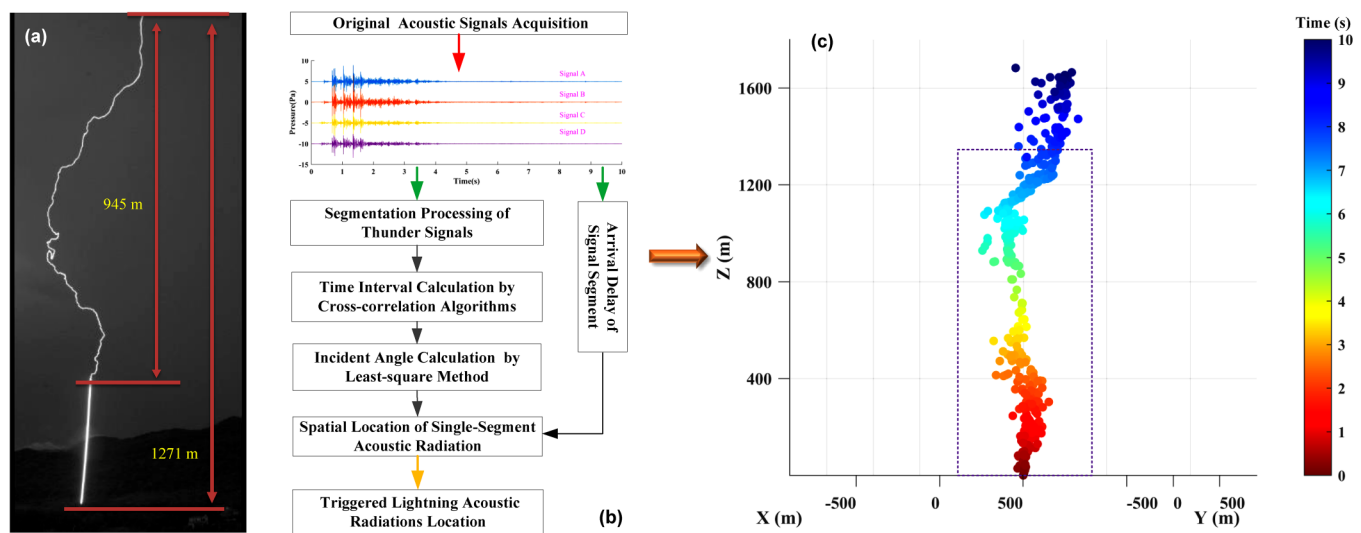
FIG. 9. (a) The image of the optical channel labeled with the estimated height. (b) Flow chart of the algorithm of acoustic radiation localization. (c) Results of the acoustic localization for triggered lightning.

of the return stroke channels recorded at the optical observing site 1.6 km away from the rocket launcher. Note that all the return stroke processes have nearly the same discharge plasma channel. Thus, the optical image of each return stroke seems the same and only one of them has been presented in Fig. 9. According to the spatial geometry relationship and the camera lens' parameters, the estimated total height of the channel in the visual field is 1271 m. The natural development bending channel in the upper part of the straight steel wire is 945 m.

The flow chart of the three-dimensional localization was shown in Fig. 9(b). The analyzed characteristics of acoustic waveform initiated by triggered lightning reported above guided the acoustic waveform segmentation. After the segmentation, the calculation of the accurate time difference and the incident angle of a single acoustic segment could then be implemented. The segment length and step length of the acoustic signals are adopted as 0.1 and 0.02 s in this study, respectively. The results of the three-dimensional localization below the height of 1800 m are shown in Fig. 9(c). It is illustrated that the acoustic radiation sources are mainly distributed along the channel of return strokes. The geometric structure of the reconstructed return-stroke channel is highly consistent with the synchronous optical image. The lightning channel below 400 m is distributed in a straight direction while the channel above bends over a wide range until the height reaches about 1150 m, continuing to develop upwards in a relatively vertical state.

IV. DISCUSSION

In the past, Uman *et al.* studied the characteristics of acoustic pressure signals in lightning discharge channels through the laboratory long gap discharge[26] and compared the observation with the theoretic shock-wave propagation attenuation law. Compared with his results, the measured amplitude in this study is relatively smaller due to the propagation effect of thunder radiations in air medium under a thunderstorm environment. While the amplitude measured in our study is like the acoustic observation of rocket-triggered lightning flash at 70 m in France[21] and acoustic results at 95 meters away from triggered flash in ICLRT, 2015.[22] Note that neither the indoor experiment nor the rocket-triggered lightning experiment reported before has described and analyzed the detailed complete time-domain acoustic pressure signals initiated by a complete lightning discharge process.

The first arrived acoustic N-shape waveform can be judged to originate from the bottom of the straight channel. Thus, the overlap effect of synchronous arrival of different acoustic radiations from the top curved channel is eliminated. The tortuosity of the channel above the straight channel is incalculable, while each small segment of the tortuous channel can be regarded as an independent source of acoustic radiation.[27–30] The corresponding N-shape waves show a low amplitude and serious overlap, which can be observed after the first arrived N-shape acoustic waveform.

The characteristics of the low-frequency band, behind the first arrived N-shape waveform, have been observed and investigated as a new phenomenon that hasn't been concerned in the literature. The reports on the infrasound waveforms or low-frequency components in the audible band of lightning have been reflected in the past. Holmes *et al.*[31] observed and counted natural lightning flashes and found that the peak frequency of thunder in some lightning cases is the low-frequency components. Farge and Blanc reported the results of lightning infrasound observations, and the locations of infrasound sources are determined using a 3-D localization.[32] Chum *et al.* observed infrasound pulses and electrostatic field changes initiated by lightning to discuss the generation of

infrasound sources.[33] However, the low-frequency band following the acoustic N-shape waveforms observed in this study has not been found in the research above. Our study has revealed that the transition phase, oscillation pattern, and duration of the low-frequency band have fairly typical consistency characteristics in different return stroke processes. While the amplitude of the low-frequency oscillation wave has a great linear correlation with the amplitude of the RS current.

Considering the causes of the formation of the low-frequency band, it is guessed that it may be related to the response of the measurement system itself. Meanwhile, to further analyze the formation mechanism of this part of the waveform, more observed data in subsequent work may be needed. On the other hand, this section of the waveform has a longer arrival time delay and has many weak-amplitude acoustic pressure waveforms superimposed on it, coming from higher channels, i.e., more distant sources of acoustic radiation. The analysis of the typical time-domain waveform features that appeared in this observation contributes to the segmentation, feature identification, and feature extraction of acoustic pressure waveforms in acoustic radiation localization techniques for channel reconstruction.

Abundant M-components discharge and corresponding acoustic pressure signals were also investigated in this study. According to Dayeh et al.,[22] the one-to-one correspondence of time-domain acoustic signals of M-component waveforms has not been shown clearly, since only one M-component with a fast wavefront produced corresponding recorded acoustic waveforms in their observation. Note that they agreed that the conditions required for each discharge process to create acoustic radiations are related to the characteristics of discharge pulse, e.g., wavefront, amplitude, and transfer charge. In this study, it is further found that there are no corresponding acoustic signals for the M-component with a much short time interval from the previous RS pulse, even if the wavefront is fast enough and the current amplitude is comparable to the RS pulse. Therefore, we recommends that another factor should be considered, i.e., the time interval of the discharge pulse and the previous one. If the time interval is too close, even if the discharge is intense, it may not cause the secondary plasma channel to expand sharply, since the ionization channel has not completely dissipated after the thermal expansion of the return channel. Then an obvious acoustic radiation source would not be excited and observed. The possible explanation has also been supported by the observed RS3 process, which has a too short time delay with the previous RS pulse and has no obvious acoustic pressure signals.

V. CONCLUSION

In this study, we report the characteristics of near-field acoustic pressure signals initiated from a rocket-triggered lightning flash with 13 return strokes, abundant initial continuous current pulsed, and M-components. Analyzing the complete near-field acoustic pressure signals, the near-field acoustic pressure signals from each return stroke are found to be composed of the first arrived N-shape waveform and the subsequent low-frequency acoustic waveforms.

The characteristic of the N-shape acoustic waveforms initiated from RS pulses was parametrically defined and quantitatively analyzed, with a comprehensively acoustic-electrical correlation investigation. It is found that the acoustic parameters related to amplitude intensity, such as P_{1max}, P_{1min}, P_{2max}, and E_{vol}, and the time parameters, such as T_r, T_d, and T_{1min}, have an obvious linear relationship with the electrical parameter I_{max} of the current pulse. Meanwhile, P_{1max} and E_{vol} have shown a linear relationship with the integral of RS current pulse. A similar correlation has also been found in the peak value of the low-frequency acoustic waveform vs I_{max}.

The low-frequency oscillating acoustic waveforms behind the first-arrived acoustic N-shape waveforms are observed as a new phenomenon. The transition phase, oscillation pattern, and duration of the low-frequency oscillating waveforms are found to have fairly typical consistency characteristics in different return-stroke processes. While the amplitude of the oscillating waveforms has a great linear correlation with the amplitude of the RS current.

The acoustic characteristics of the ICC pulses have also been measured and discussed. Due to the complexity of ICC current pulses observed in this flash, the one-to-one correspondence of acoustic and electrical pulses is not as clear as in the other discharge processes. Furthermore, abundant M-components and their acoustic pressure signals have been investigated. It is found that the too-close time interval between M-component and previous current pulses significantly affects the generation and response of the acoustic pressure signals from this process, even though the current amplitude is comparable to that of the return stroke pulse and the wavefront is fast. The same phenomenon has also been observed in the acoustic signals from a return stroke pulse with a too close interval from the previous pulse.

Based on the acoustic array measurement, the acoustic source localization with great accuracy for lightning channel reconstruction was realized. The reconstructed channel structure agrees with the synchronously-captured optical image. Further research on the technique of acoustic radiation localization will be carried out.

AUTHOR DECLARATIONS

Conflict of Interest

The authors have no conflicts to disclose.

Author Contributions

Jianguo Wang: Funding acquisition (equal); Investigation (equal); Methodology (equal); Project administration (equal); Supervision (equal); Validation (equal). **Jinxin Cao:** Data curation (equal); Formal analysis (equal); Investigation (equal); Methodology (equal); Writing – original draft (equal); Writing – review & editing (equal). **Li Cai:** Investigation (equal); Project administration (equal); Supervision (equal); Writing – review & editing (equal). **Rui Su:** Data curation (equal); Methodology (equal). **Mi Zhou:** Methodology (equal); Writing – review & editing (equal). **Yadong**

06 January 2025 07:00:25

Fan: Supervision (equal); Writing – review & editing (equal).
Quanxin Li: Visualization (equal).

DATA AVAILABILITY

The data that support the findings of this study are available from the corresponding author upon reasonable request.

REFERENCES

[1]V. A. Rakov and M. A. Uman, *Lightning: Physics and Effects* (Cambridge University Press, 2007).
[2]J. A. Bodhika, W. G. Dharmarathna, M. Fernando, and V. Cooray, "A preliminary study on characteristics of thunder pulses of lightning," in *2014 International Conference on Lightning Protection (ICLP)* (IEEE, 2014). pp. 260–264.
[3]J. A. Bodhika, W. G. Dharmarathna, M. Fernando, and V. Cooray, "Characteristics of thunder pertinent to tropical lightning," in *2018 34th International Conference on Lightning Protection (ICLP)* (IEEE, 2018) pp. 1–5.
[4]J. Cao, J. Wang, H. Qin, J. Dai, R. Su, and L. Cai, "Acoustic observation of a lightning flash attached to a wind turbine," in *2018 XVI International Conference on Atmosphere Electricity (ICAE)* (2018), pp. 1–8.
[5]H. E. Bass and R. E. Losey, "Effect of atmospheric absorption on the acoustic power spectrum of thunder," J. Acoust. Soc. Am. **57**, 822–823 (1975).
[6]H. E. Bass, "The propagation of thunder through the atmosphere," J. Acoust. Soc. Am. **67**, 1959–1966 (1980).
[7]L. J. Gallin, M. Rénier, E. Gaudard, T. Farges, R. Marchiano, and F. Coulouvrat, "One-way approximation for the simulation of weak shock wave propagation in atmospheric flows," J. Acoust. Soc. Am. **135**(5), 2559–2570 (2014).
[8]O. Yuhua and Y. Ping, "Audible thunder characteristic and the relation between peak frequency and lightning parameters," J. Earth Syst. Sci. **121**, 211–220 (2012).
[9]L. J. Gallin, T. Farges, R. Marchiano, F. Coulouvrat, E. Defer, W. Rison, W. Schulz, and M. Nuret, "Statistical analysis of storm electrical discharges reconstituted from a lightning mapping system, a lightning location system, and an acoustic array," J. Geophys. Res. Atmos. **121**, 3929–3953, https://doi.org/10.1002/2015JD023745 (2016).
[10]S. Qiu, B. Zhou, and L. Shi, "Synchronized observations of cloud-to-ground lightning using VHF broadband interferometer and acoustic arrays," J. Geophys. Res. **117**(D19204), 1–9 (2012).
[11]H. Zhang, S. Gu, J. Chen, C. Zhao, M. Wu, B. Yan *et al.*, "Single-station-based lightning mapping system with electromagnetic and thunder signals," IEEE Trans. Plasma Sci. **47**, 1421–1428 (2019).
[12]R. Arechiga, M. Stock, R. Thomas, H. Erives, W. Rison, H. Edens *et al.*, "Location and analysis of acoustic infrasound pulses in lightning," Geophys. Res. Lett. **41**, 4735–4744, https://doi.org/10.1002/2014GL060375 (2014).
[13]V. A. Rakov and M. A. Uman, *Lightning: Physics and Effects* (Cambridge University Press, New York, 2003).
[14]L. Cai, J. Li, J. Wang, R. Su, F. Wang, and Q. Li, "Optical progressing and electric field change characteristics of altitude—Triggered lightning flash with different development paths," J. Geophys. Res. Atmos. **126**, 1–16, https://doi.org/10.1029/2020JD033774 (2021).

[15]L. Cai, J. Li, J. Wang, R. Su, Y. Ke, M. Zhou, and Q. Li, "Differences between flashes with and without return strokes in rocket-triggered lightning," Geophys. Res. Lett. **48**, 1–8, https://doi.org/10.1029/2021GL093483 (2021).
[16]J. Wang, S. Wang, L. Cai, D. Lu, Q. Li, M. Zhou *et al.*, "Observation of induced voltage at the terminal of 10 kV distribution line by nearby triggered lightning," IEEE Trans. Power Deliv. **35**, 1968–1976 (2020).
[17]W. Jianguo, Y. Zhao, Y. Fang, L. Cai, W. Shoupeng, Z. Xu *et al.*, "Observation of overvoltage at the terminal of 10 kV distribution line by direct triggered lightning," IEEE Trans. Power Deliv. (published online, 2021).
[18]F. Wang, J. Wang, L. Cai, R. Su, W. Ding, and Z. Xu, "Leader-chasing behavior in negative artificial triggered lightning flashes," Sci. Rep. **11**, 11598 (2021).
[19]Bhartendu, "A study of atmospheric pressure variations from lightning discharges," Can. J. Phys. **46**, 269–281 (1968).
[20]N. O. Ajayi, "Acoustic observation of thunder from cloud-ground flashes," J. Geophys. Res. **77**, 4586–4587, https://doi.org/10.1029/JC077i024p04586 (1972).
[21]P. Depasse, "Lightning acoustic signature," J. Geophys. Res. **99**, 25933–25940, https://doi.org/10.1029/94JD01986 (1994).
[22]M. A. Dayeh, N. D. Evans, S. A. Fuselier, J. Trevino, J. Ramaekers, J. R. Dwyer *et al.*, "First images of thunder: Acoustic imaging of triggered lightning," Geophys. Res. Lett. **42**, 6051–6057, https://doi.org/10.1002/2015GL064451 (2015).
[23]L. Yun, X. Xiaochun, L. Bin, and P. Jinfeng, "Time-frequency analysis based on the s-transform," Int. J. Signal Process. Image Process. Pattern Recognit. **6**, 245–254 (2013).
[24]J. Wang, J. Cao, L. Cai, Y. Fan, M. Zhou, and Q. Li, *Characteristics of Acoustic Response From Simulated Impulsive Lightning Current Discharge* (High Voltage, 2019).
[25]R. Jiang, X. Qie, J. Yang, C. Wang, and Y. Zhao, "Characteristics of M-component in rocket-triggered lightning and a discussion on its mechanism," Radio Sci. **48**, 597–606 (2013).
[26]M. A. Uman, A. H. Cookson, and J. B. Moreland, "Shock wave from a four-meter spark," J. Appl. Phys. **41**, 3148–3155 (1970).
[27]A. A. Few, "Power spectrum of thunder," J. Geophys. Res. **74**, 6926–6934, https://doi.org/10.1029/JC074i028p06926 (1969).
[28]A. A. Few, "Lightning channel reconstruction from thunder measurements," J. Geophys. Res. **75**, 7517–7523, https://doi.org/10.1029/JC075i036p07517 (1970).
[29]A. A. Few, "Thunder signatures," Eos, Trans. Am. Geophys. Union **55**, 508–514 (1974).
[30]H. S. Ribner and D. Roy, "The acoustics of thunder: A quasilinear model for tortuous lightning," J. Acoust. Soc. Am. **72**, 1911–1925 (1982).
[31]C. R. Holmes, M. Brook, P. Krehbiel, and R. Mccrory, "On the power spectrum and mechanism of thunder," J. Geophys. Res. **76**, 2106–2115, https://doi.org/10.1029/JC076i009p02106 (1971).
[32]T. Farges and E. Blanc, "Characteristics of infrasound from lightning and sprites near thunderstorm areas," J. Geophys. Res.: Space Phys. **115**, 1–7, https://doi.org/10.1029/2009JA014700 (2010).
[33]J. Chum, G. Diendorfer, T. Šindelářová, J. Baše, and F. Hruska, "Infrasound pulses from lightning and electrostatic field changes: Observation and discussion," J. Geophys. Res. Atmos. **118**, 10653–10664, https://doi.org/doi:10.1002/jgrd.50805 (2013).

06 January 2025 07:00:25